Supplementary Information

Bioinspired light-driven water surface jumper with record high jumping performance that transcends the biological jumping limit

Changsong Zhan[1,2,†], Zhen Hou[1,†], Zhaomin Chen[1,3,†], Naizheng Tan[4,†], Jiwei Jiang[1,†,*], BinChi Zhang[1], Chenjun Chu[1], A-Man Zhang[4,5], Hui Zhang[1,*], Bin Dong[1,*], Lifeng Chi[1,*], Metin Sitti[3,*]

[1]State Key Laboratory of Bioinspired Interfacial Materials Science, Jiangsu Key Laboratory for Carbon-based Functional Materials and Devices and Institute of Functional Nano and Soft Materials (FUNSOM), Soochow University, Suzhou 215123, China.

[2]Suzhou Laboratory, Suzhou 215123, China.

[3]School of Medicine and College of Engineering, Koç University, 34450 Istanbul, Turkey.

[4]Nanhai Institute of Harbin Engineering University, Sanya 572024, China.

[5]College of Shipbuilding Engineering, Harbin Engineering University, 150001 Harbin, China.

[†]These authors contributed equally to this work: Changsong Zhan, Zhen Hou, Zhaomin Chen, Naizheng Tan, Jiwei Jiang.

[*]Corresponding authors. E-mail: msitti@ku.edu.tr; chilf@suda.edu.cn; bdong@suda.edu.cn; huizhang@suda.edu.cn; jwjiang@suda.edu.cn

Supplementary Table 1. Comparison of the jumping performance, the photothermal temperature of different polypyrrole (PPy) derivatives/polyvinyl alcohol (PVA) based jumpers and the energy gap of substituted PPy.

Jumper	Monomer	Jumping height (cm)	Photothermal temperature (°C)	Energy gap of substituted PPy (eV)
PPy/PVA	Pyrrole	62	137.4	1.22
Me-PPy/PVA	1-Methylpyrrole	72.8	164.3	1.05
CHO-PPy/PVA	1H-Pyrrole-3-carbaldehyde	51.3	107.4	1.30
Ph-PPy/PVA	1-Phenylpyrrole	57.6	121.1	1.28
CN-PPy/PVA	1H-Pyrrole-2-carbonitrile	0	48	2.22
NO_2-PPy/PVA	3-Nitropyrrole	0	85	1.96

Supplementary Figures:

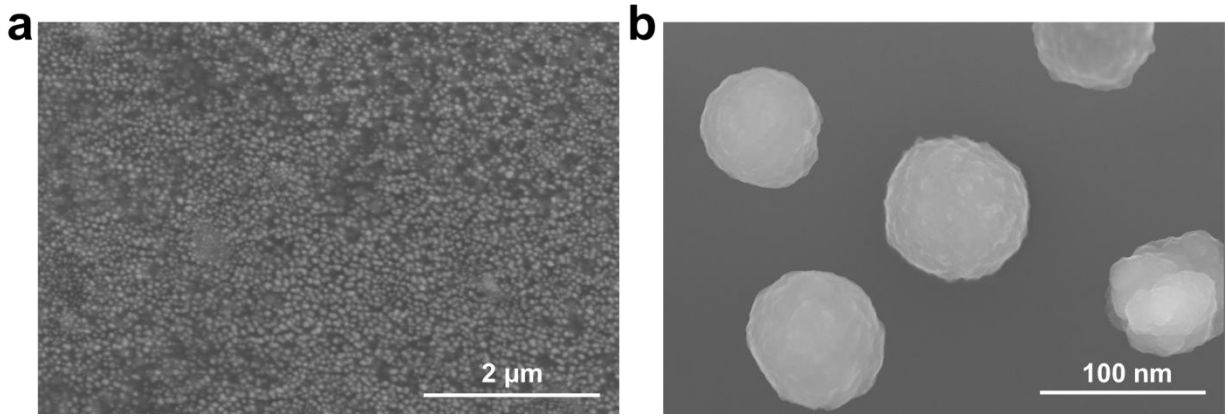

Supplementary Figure 1. (a,b) The scanning electron microscope (SEM) image showing the Me-PPy nanoparticles.

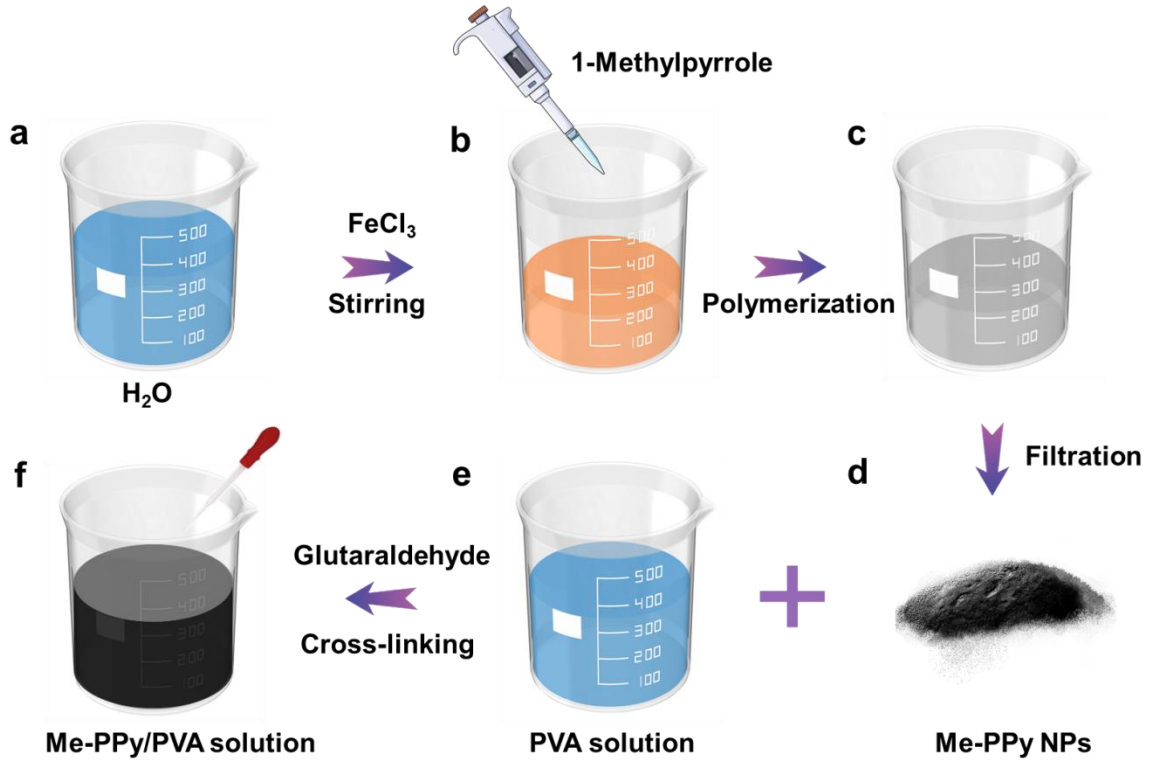

Supplementary Figure 2. (a-f) Schematic illustrating the preparation of the Me-PPy/PVA solution.

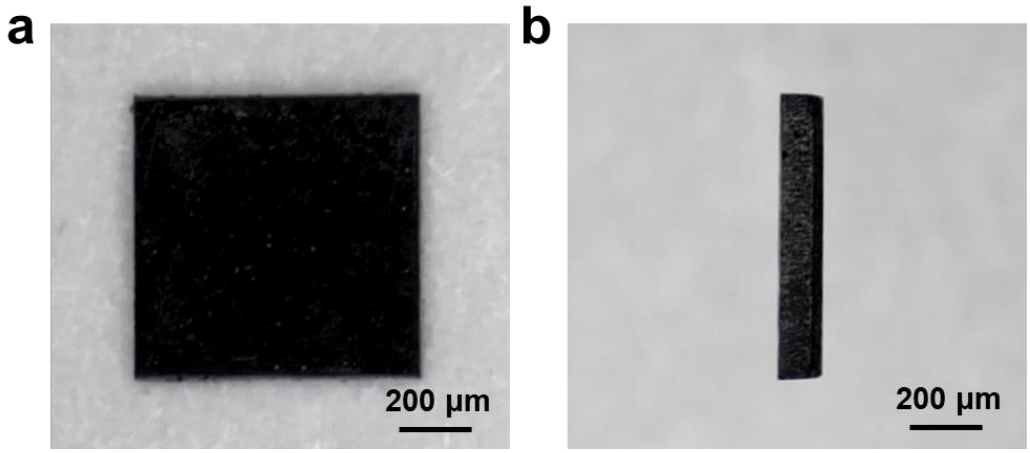

Supplementary Figure 3. (a) Top and (b) side view optical images showing the jumper consisting of Me-PPy/PVA composite.

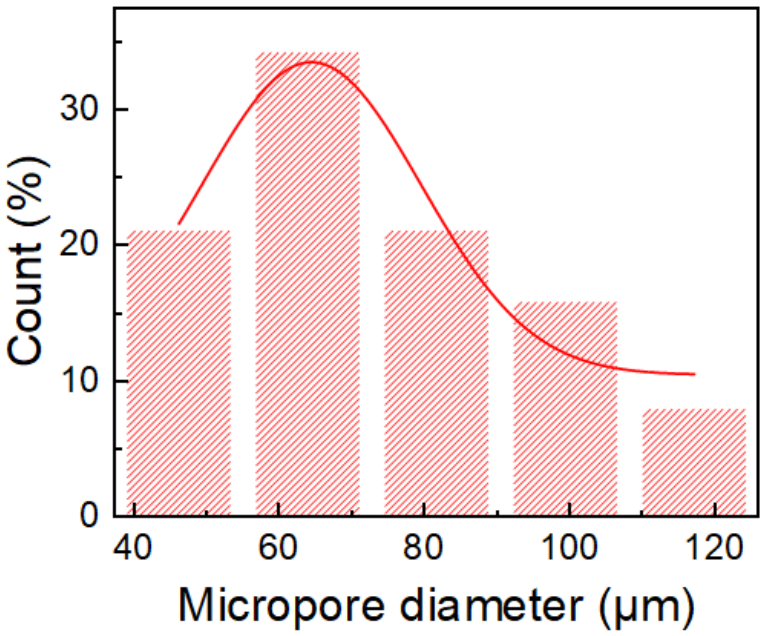

Supplementary Figure 4. Average micropore diameter on the surface of the light-driven jumper.

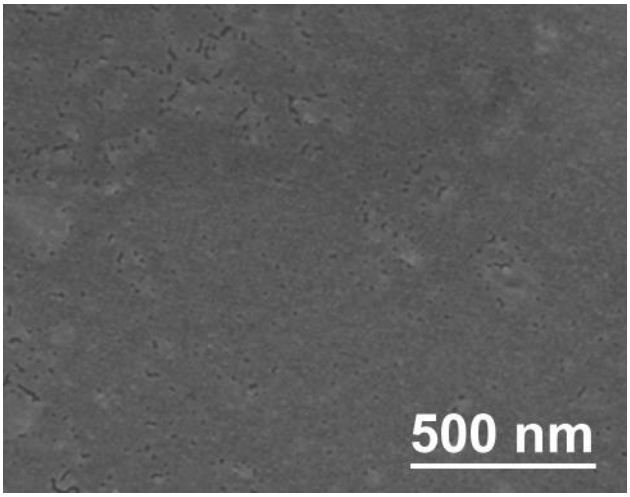

Supplementary Figure 5. The scanning electron microscope (SEM) image showing the morphology of the area other than the micropores on the surface of the light-driven jumper.

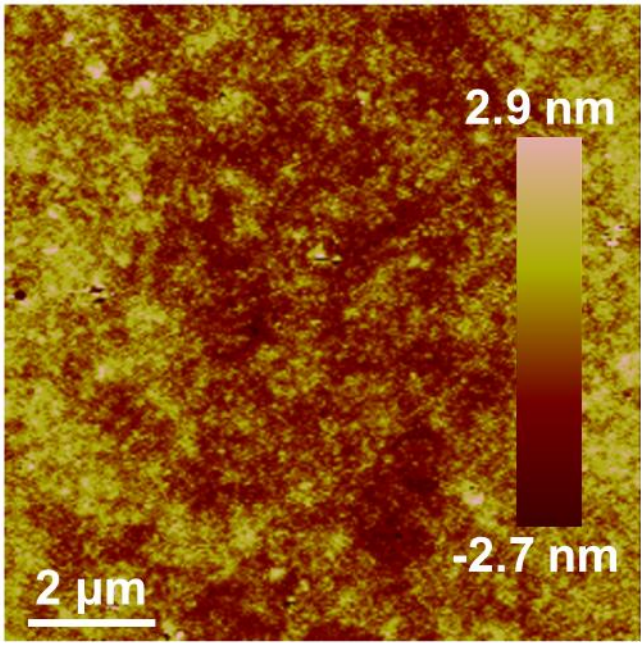

Supplementary Figure 6. The atomic force microscopy (AFM) image showing the morphology of the area other than the micropores on the surface of the light-driven jumper.

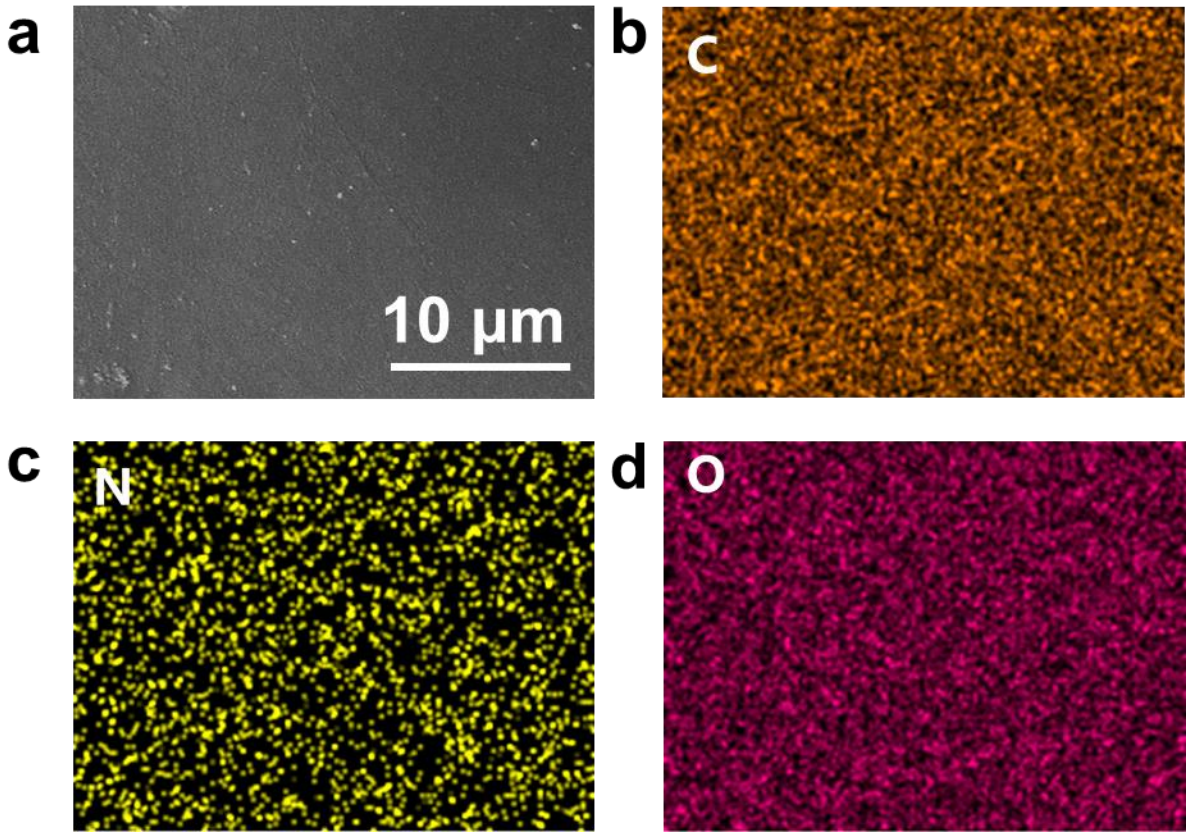

Supplementary Figure 7. (a) SEM image and the corresponding energy-dispersive X-ray (EDX) analysis of (b) carbon, (c) nitrogen, and (d) oxygen elements on the surface of the light-driven jumper.

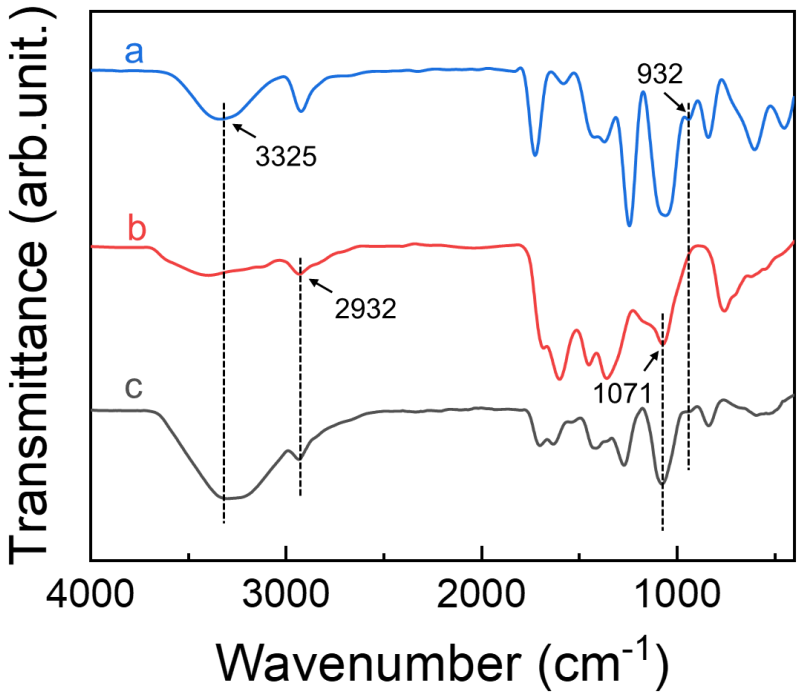

Supplementary Figure 8. Fourier transform infrared spectroscopy (FTIR) measurement of (a) PVA, (b) Me-PPy and (C) the Me-PPy/PVA composite.

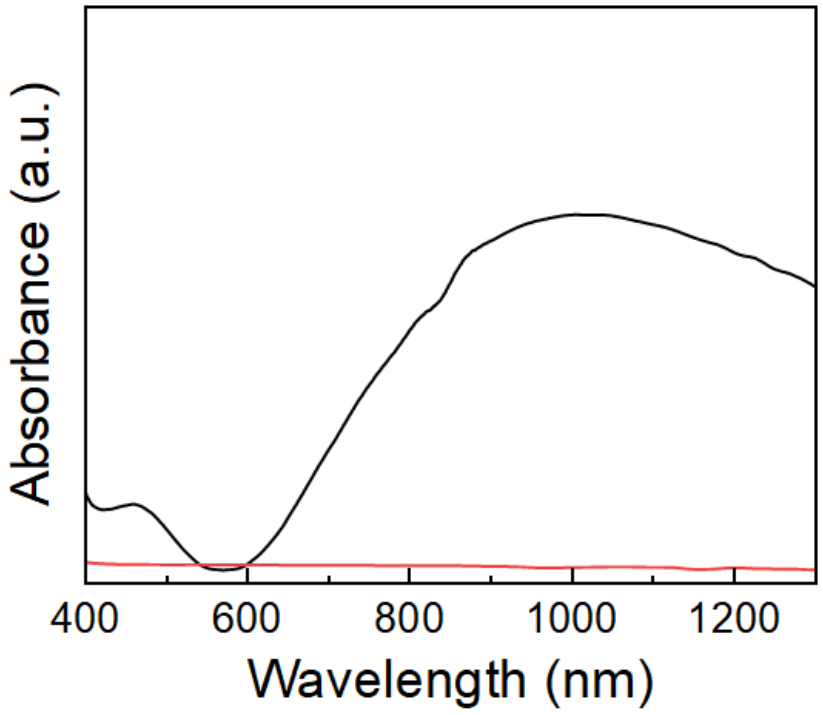

Supplementary Figure 9. The ultraviolet visible near-infrared (UV-Vis-NIR) spectra of the Me-PPy/PVA composite (black curve) and PVA (red curve).

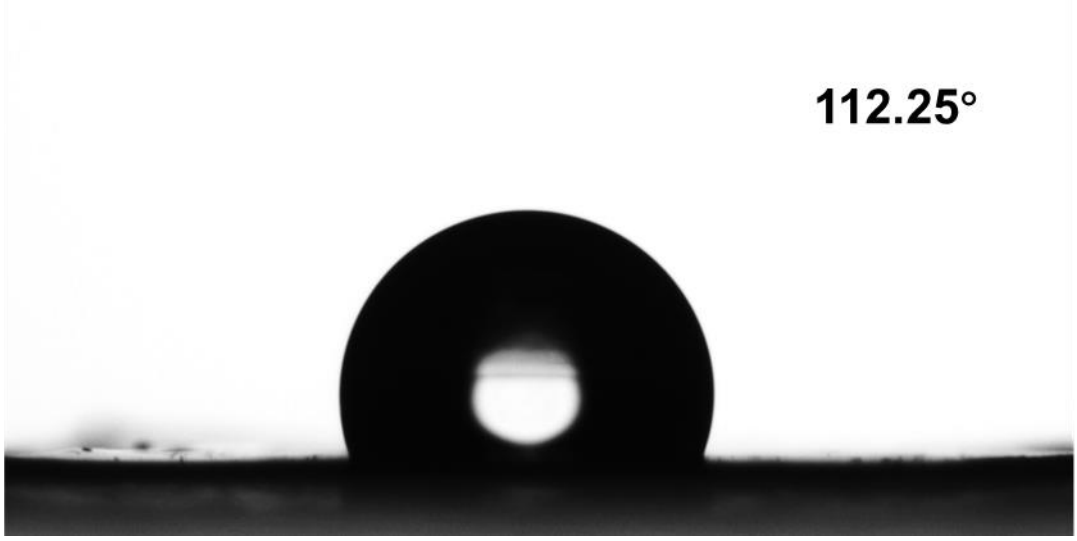

Supplementary Figure 10. The water contact angle on the surface of the Me-PPy/PVA composite film with micropores.

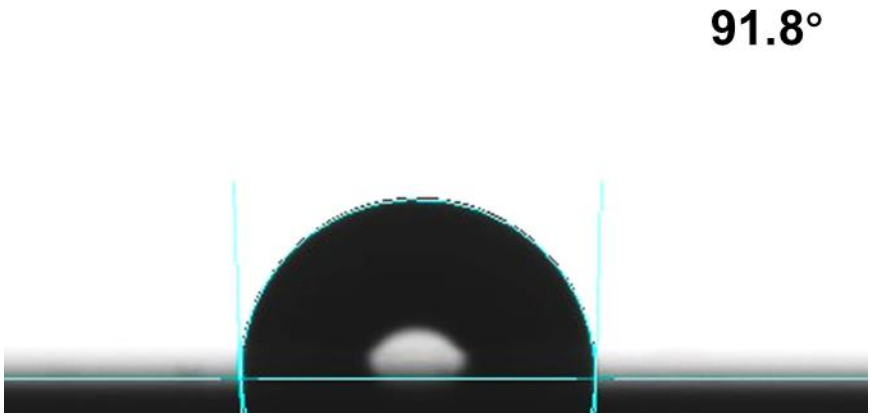

Supplementary Figure 11. The water contact angle on the surface of the Me-PPy/PVA composite film without micropores.

Supplementary Figure 12. CCD image illustrating a water droplet on a vertically aligned Me-PPy/PVA composite film. The droplet does not slide or roll off.

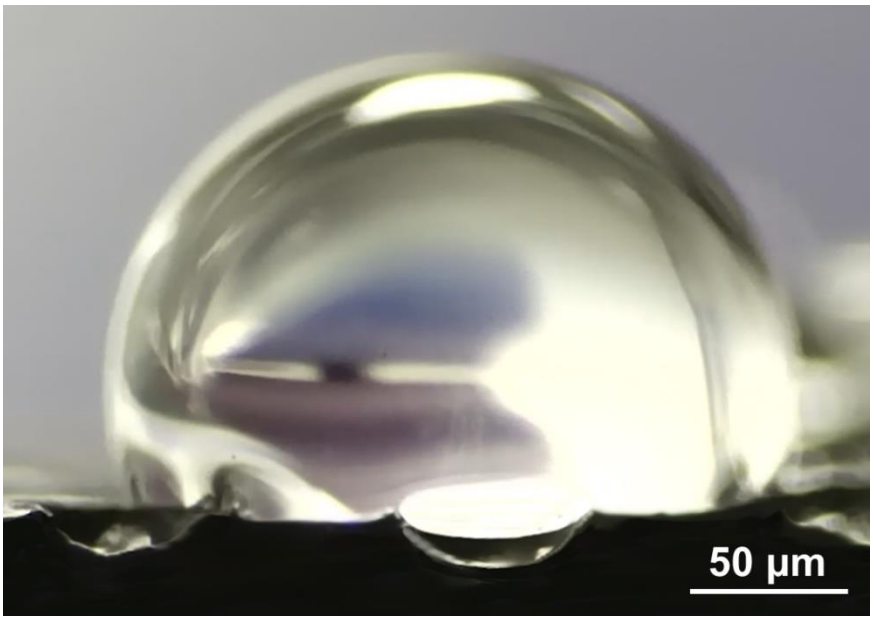

Supplementary Figure 13. CCD image showing the water droplet on the surface of the Me-PPy/PVA composite film. The partial wetting of the micropores indicates the surface wetting state between the Wenzel and Cassie states.

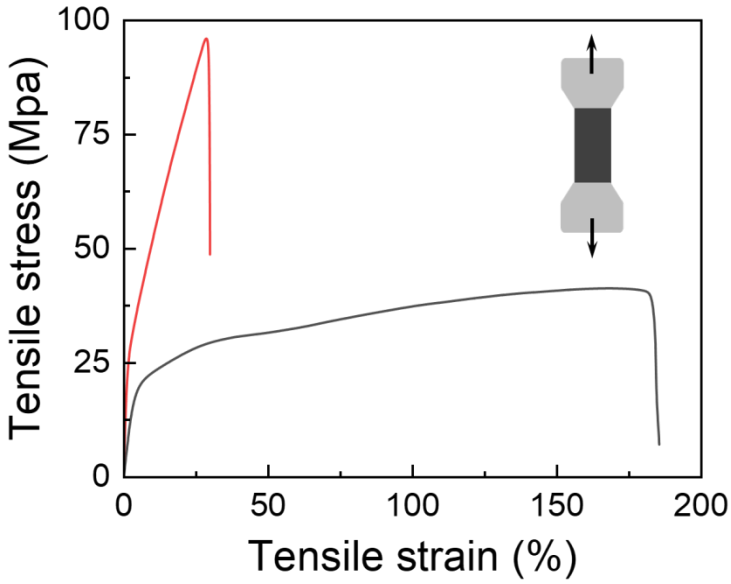

Supplementary Figure 14. Tensile stress-strain curves of the Me-PPy/PVA composite film (red curve) and the crosslinked PVA film (black curve). Inset: Schematic illustration showing the tensile test.

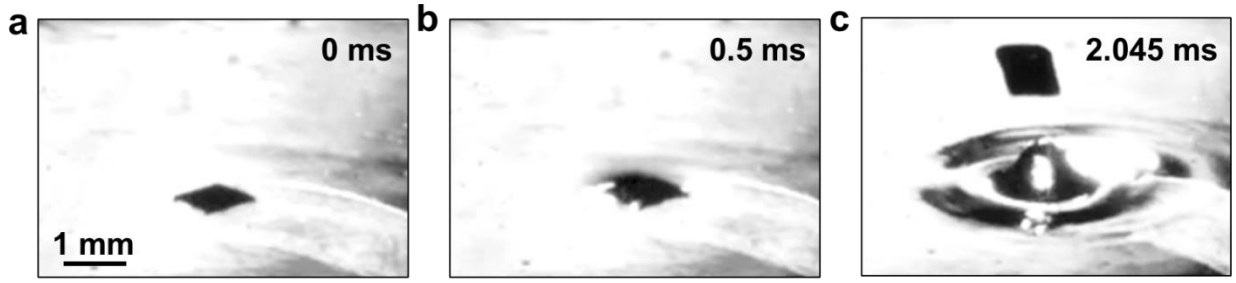

Supplementary Figure 15. (a-c) A series of images recorded by high-speed camera showing the water surface jumping motion of the light-driven jumper. These images are captured from Supplementary Movie 1.

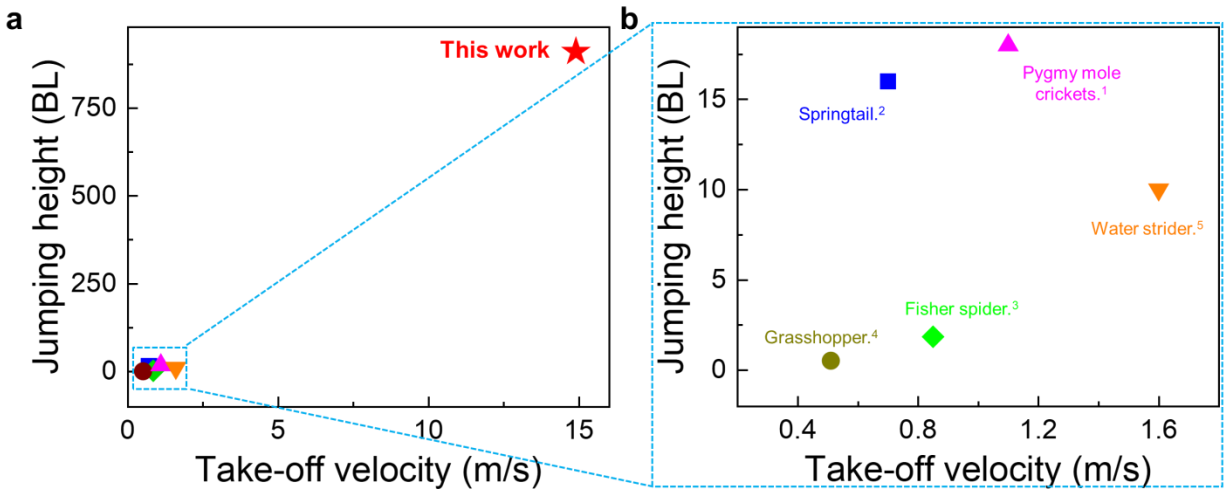

Supplementary Figure 16. (a) Comparison of the water surface jumping height and take-off velocity between the light-driven jumper in the current study and the biological counterparts reported in the literatures. (b) Magnified view of the blue dotted rectangle shown in (a)[1-5].

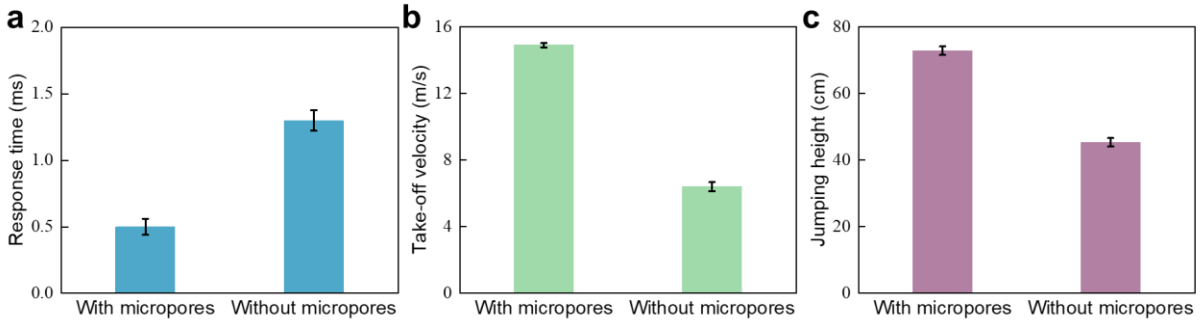

Supplementary Figure 17. Comparison of (a) the response time, (b) the take-off velocity, and (c) the jumping height of light-driven jumpers with and without surface micropores.

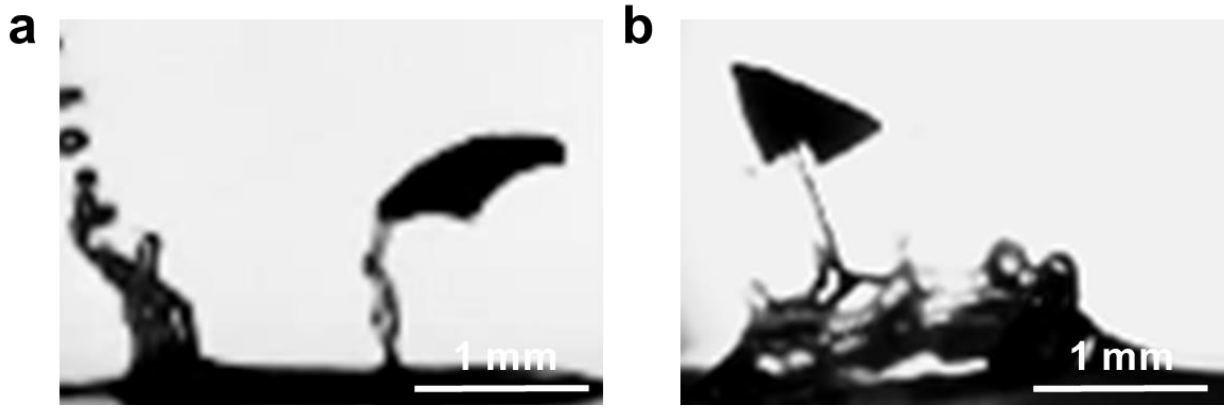

Supplementary Figure 18. High-speed camera images of (a) Me-PPy/Gelatin and (b) Me-PPy/HPC based jumpers, showing obvious deformation during the jumping process.

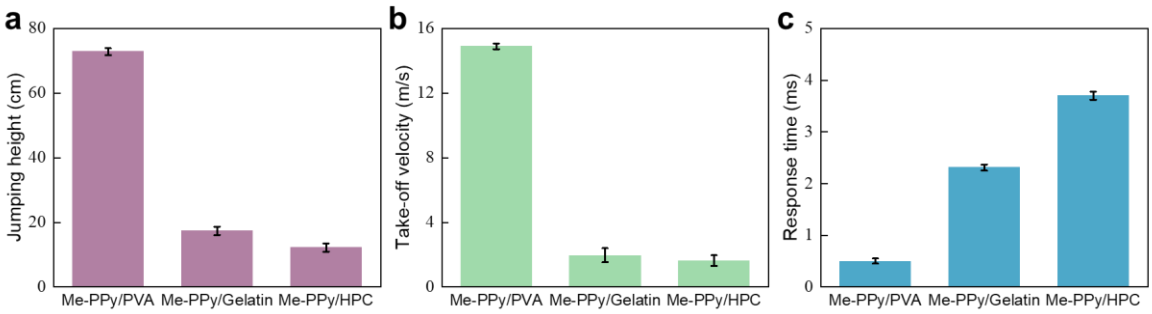

Supplementary Figure 19. Comparison of (a) the jumping height, (b) the take-off velocity, and (c) the response time of different light-driven jumpers consisting Me-PPy/PVA, Me-PPy/Gelatin and Me-PPy/HPC, respectively. Error bars represent standard deviations.

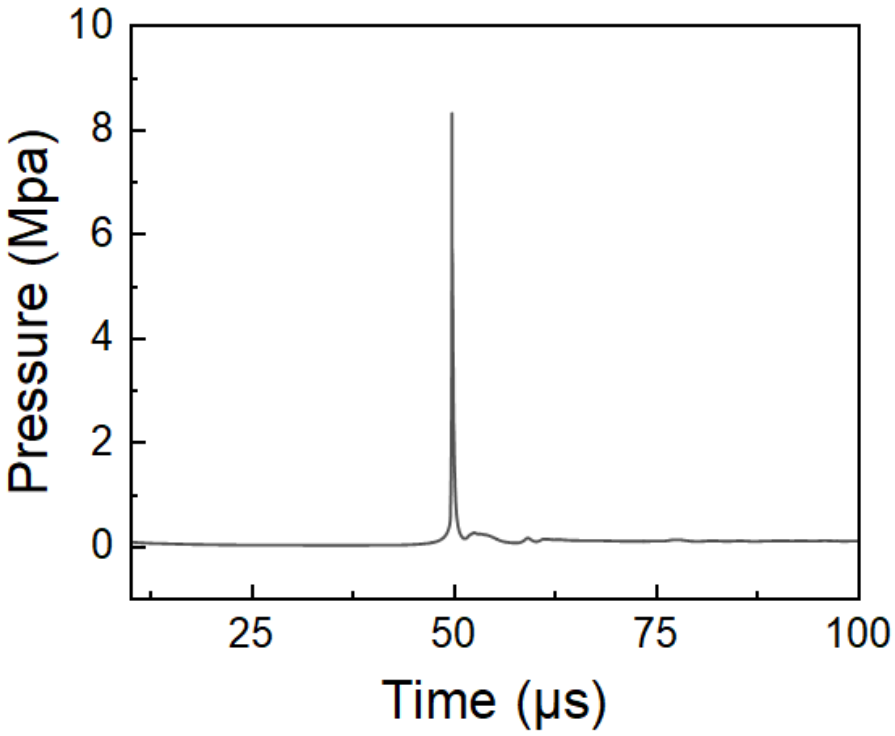

Supplementary Figure 20. The simulated curve showing the bubble pressure applied on the light-driven jumper as a function of time.

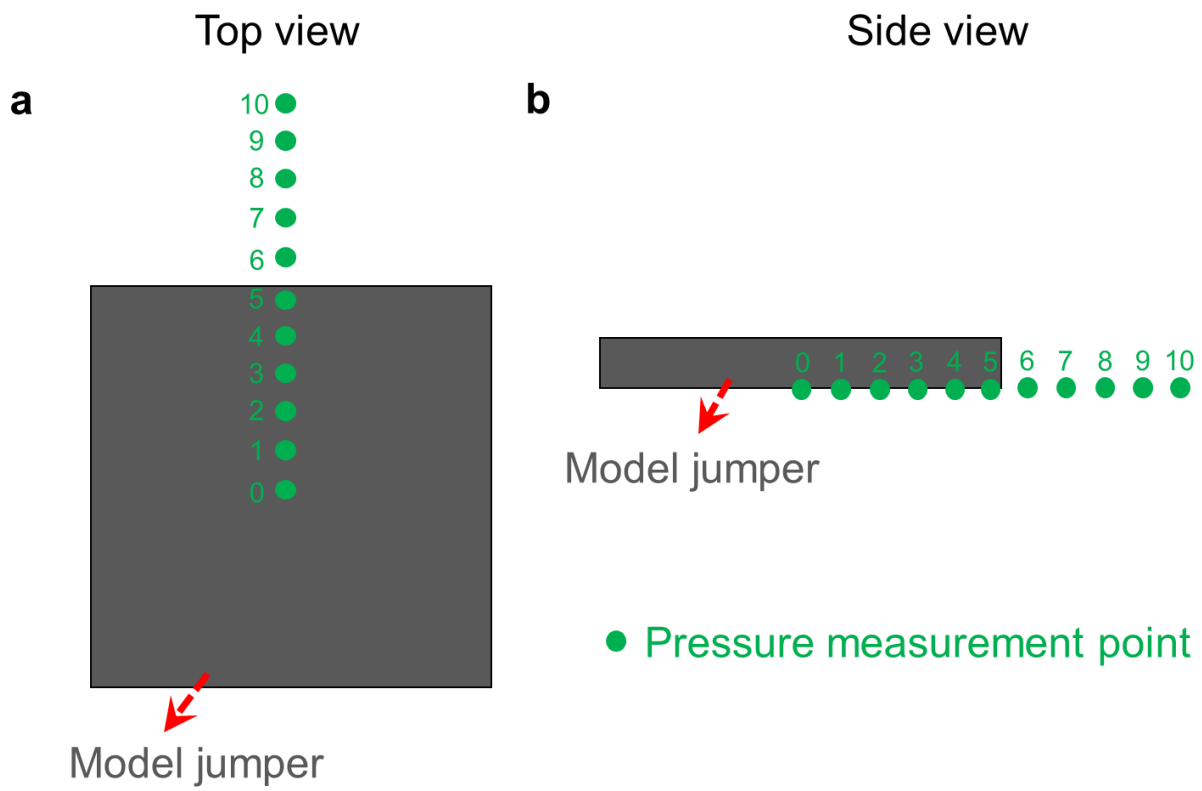

Supplementary Figure 21. (a) Top and (b) side view diagrams of the simulation model which show the position of the pressure measuring point. Note that 11 measuring points are set equidistantly from each other with 6 on the plate and 5 off the plate.

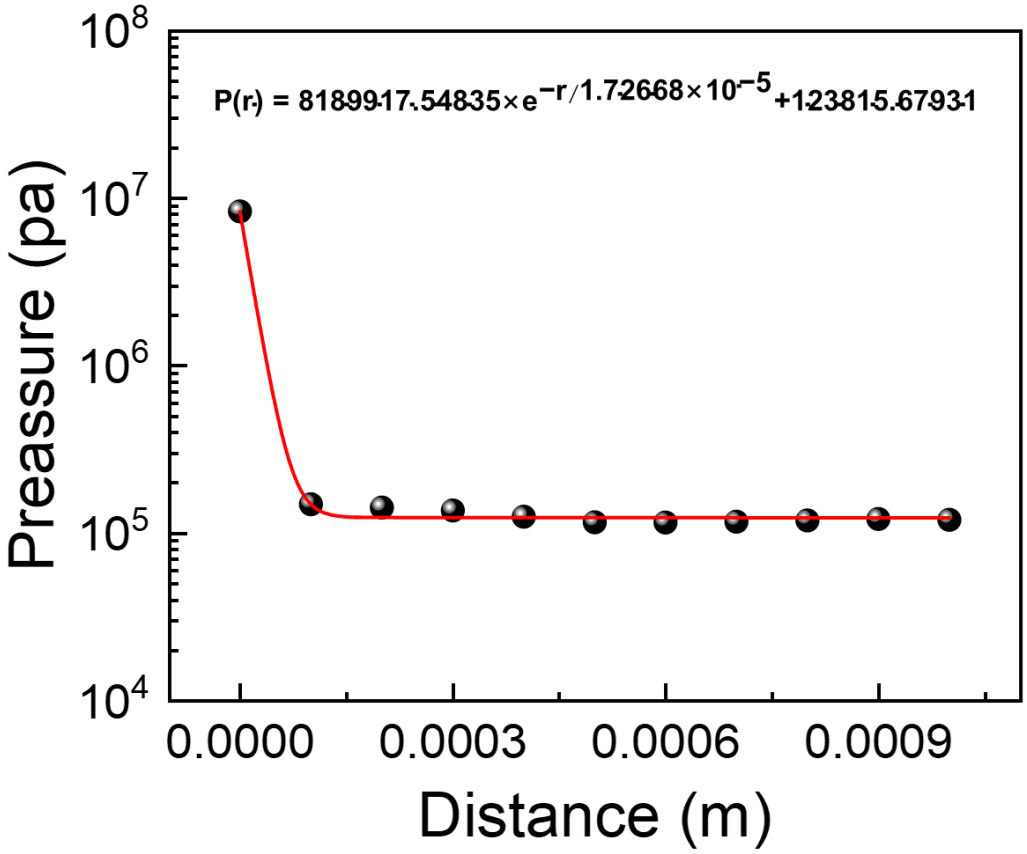

Supplementary Figure 22. The simulated pressure at 11 pressure measurement points shown in Supplementary Figure 21 at the moment of bubble bursting (black dots) and the fitted decay curve (the red curve).

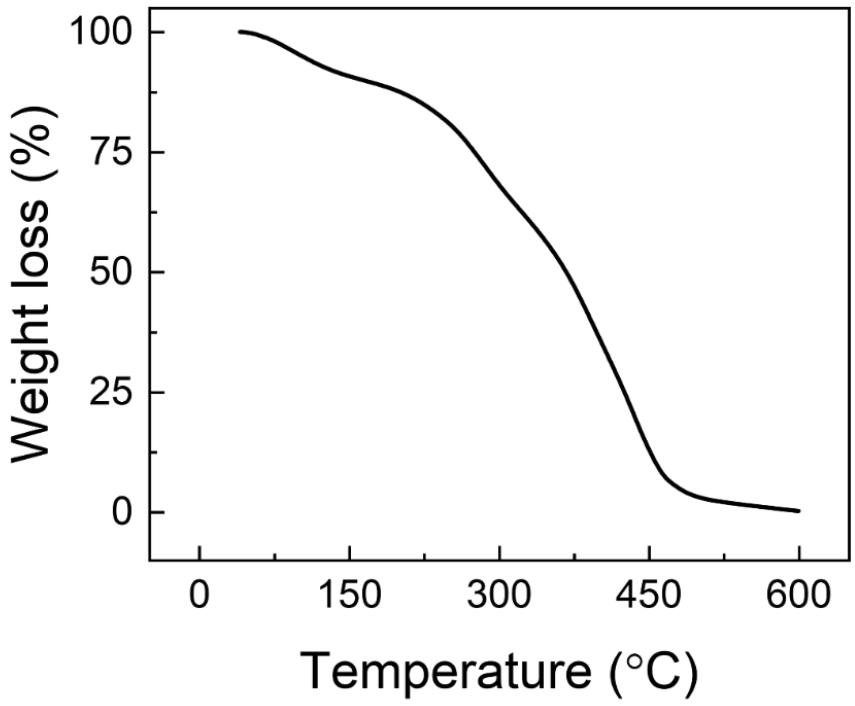

Supplementary Figure 23. The thermogravimetric analysis (TGA) curve of the Me-PPy/PVA composite.

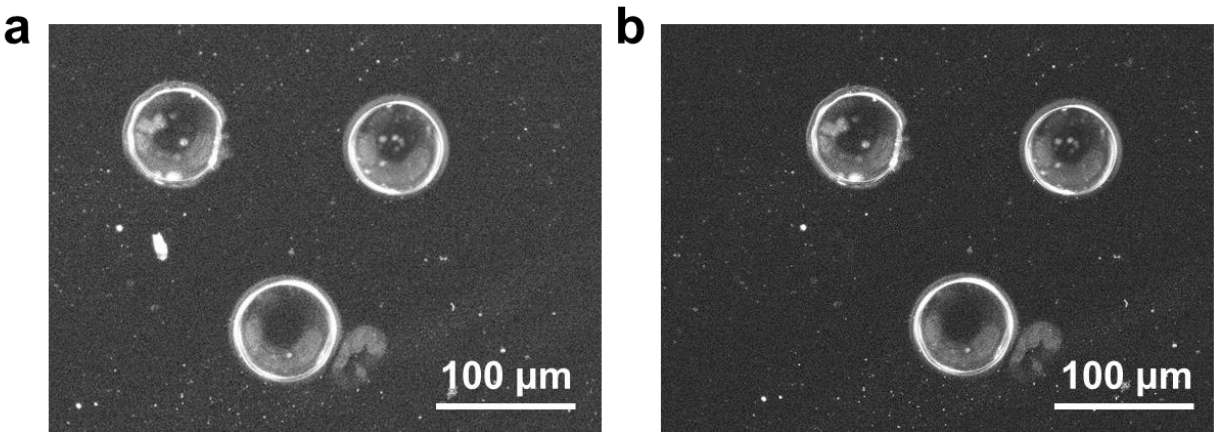

Supplementary Figure 24. Optical microscopic images showing the surface morphology of the light-driven jumper (a) before and (b) after the light actuation. There are negligible changes in the surface morphology.

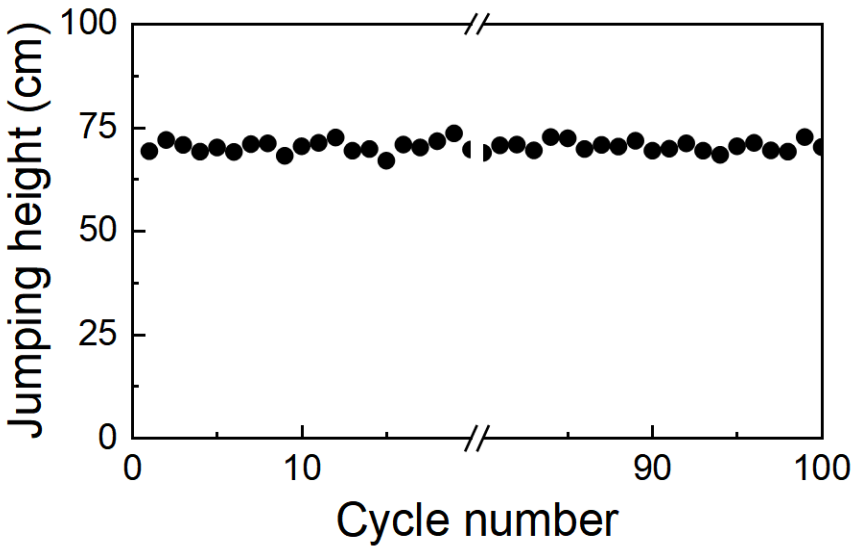

Supplementary Figure 25. The jumping performance of the Me-PPy/PVA based jumper upon the repetitive light actuation.

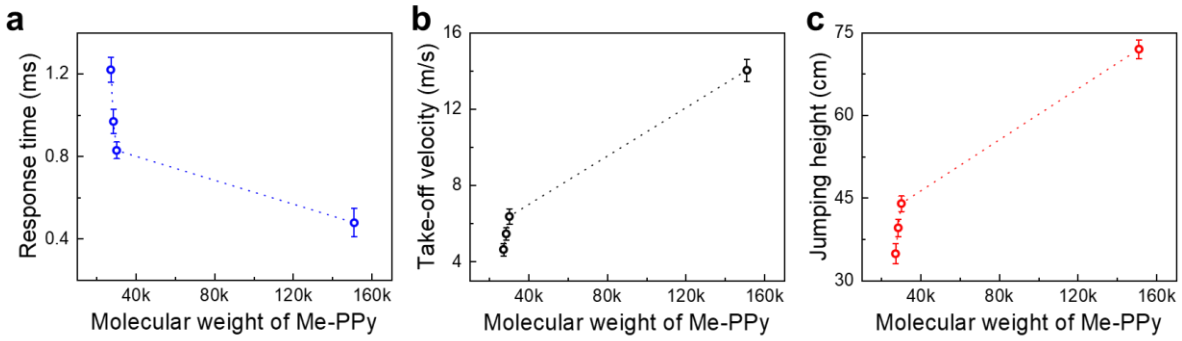

Supplementary Figure 26. The influence of the molecular weight of Me-PPy on (a) the response time, (b) the take-off velocity and (c) the jumping height of the light-driven Me-PPy/PVA based jumper. Error bars denote the standard deviation.

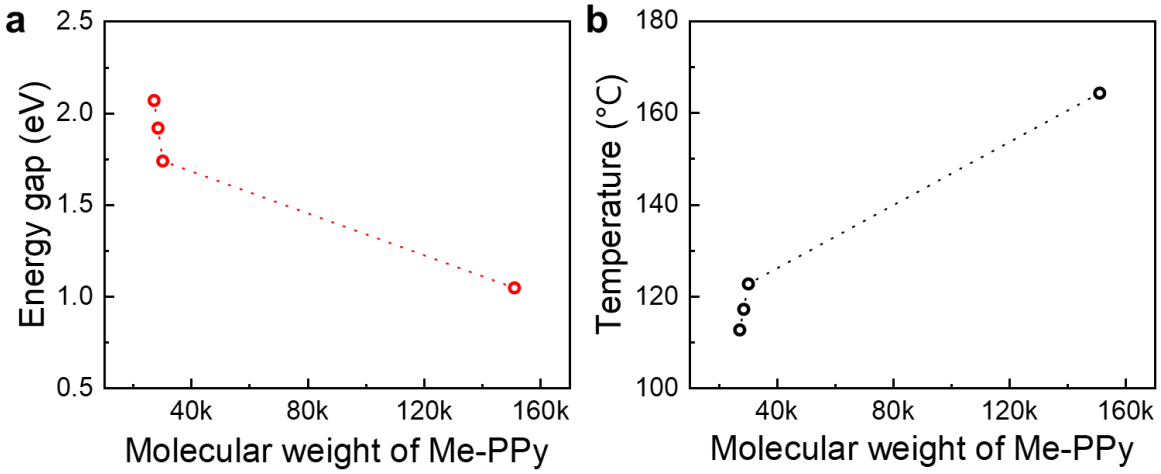

Supplementary Figure 27. (a) Energy gap and (b) the photothermal temperature of Me-PPy with different molecular weight.

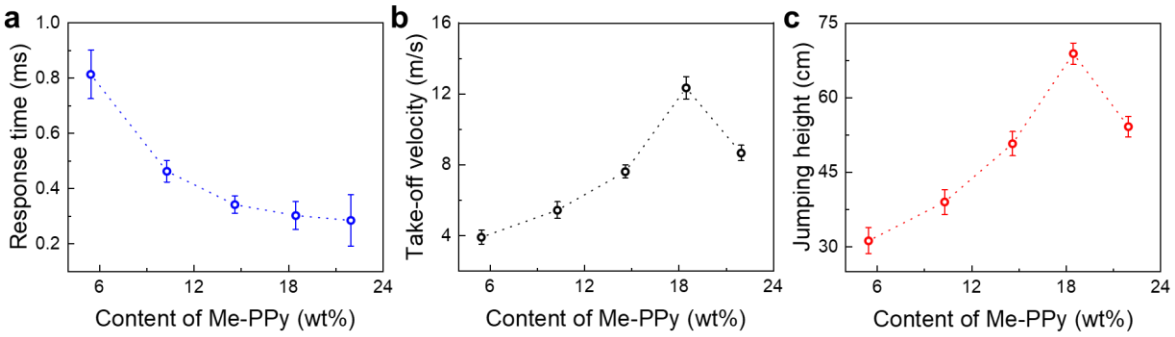

Supplementary Figure 28. The effect of the Me-PPy content on (a) the response time, (b) the take-off velocity and (c) the jumping height of the light-driven jumper. Error bars denote the standard deviation.

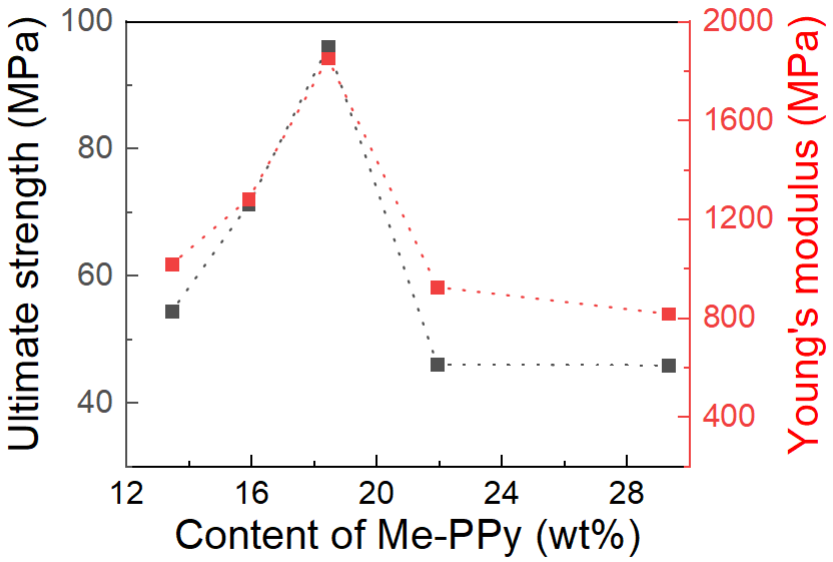

Supplementary Figure 29. The influence of the Me-PPy content on the ultimate strength and the Young's modulus of the light-driven jumper.

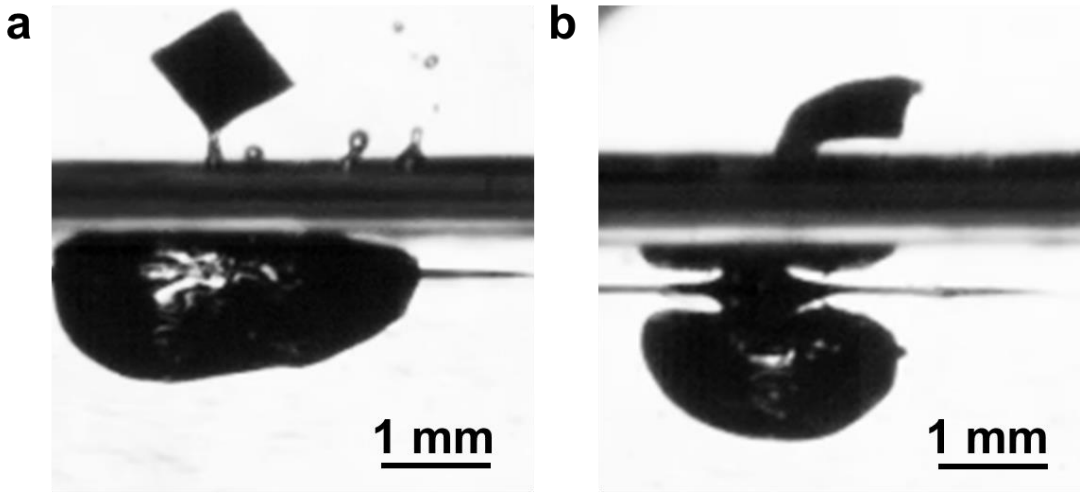

Supplementary Figure 30. The high-speed camera images showing the shape of the Me-PPy/PVA jumper with (a) 18.5% and (b) 22% Me-PPy contents during the water surface jumping process. The jumper with 22% Me-PPy content shows obvious deformation.

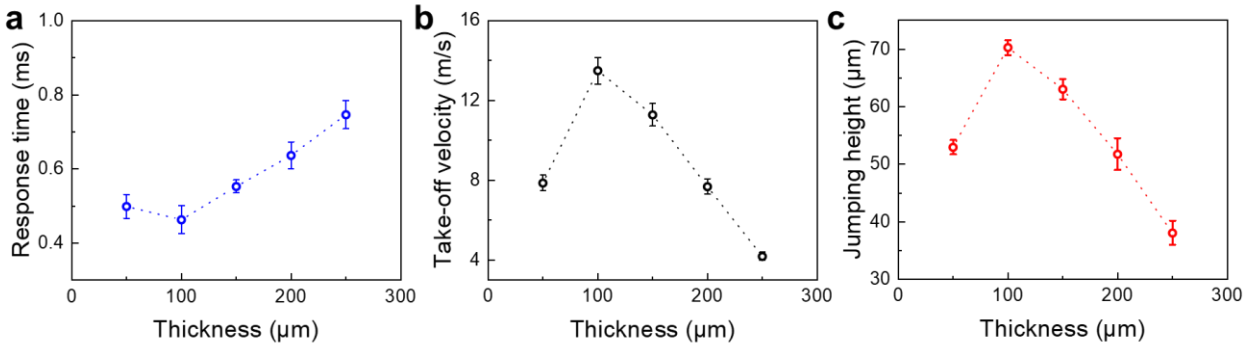

Supplementary Figure 31. The influence of the thickness of the light-driven jumper on (a) the response time, (b) the take-off velocity and (c) the jumping height of the light-driven jumper. Error bars denote the standard deviation.

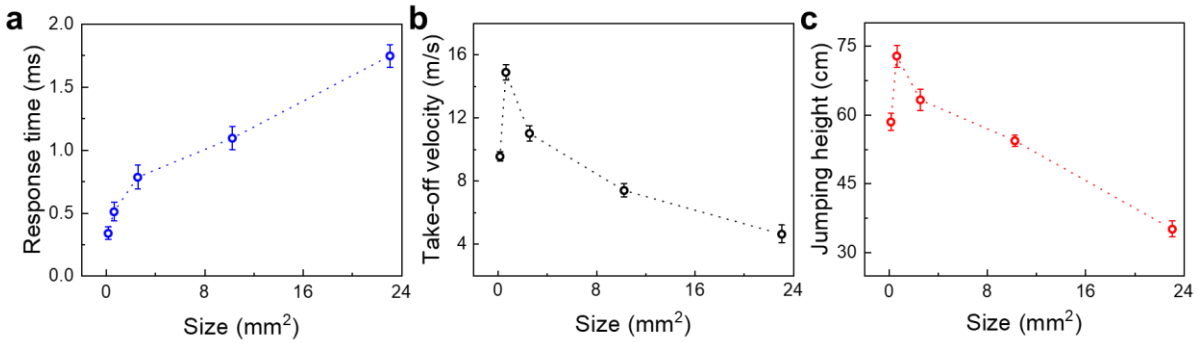

Supplementary Figure 32. The effect of the size of the light-driven jumper on (a) the response time, (b) the take-off velocity and (c) the jumping height of the light-driven jumper. Error bars denote the standard deviation.

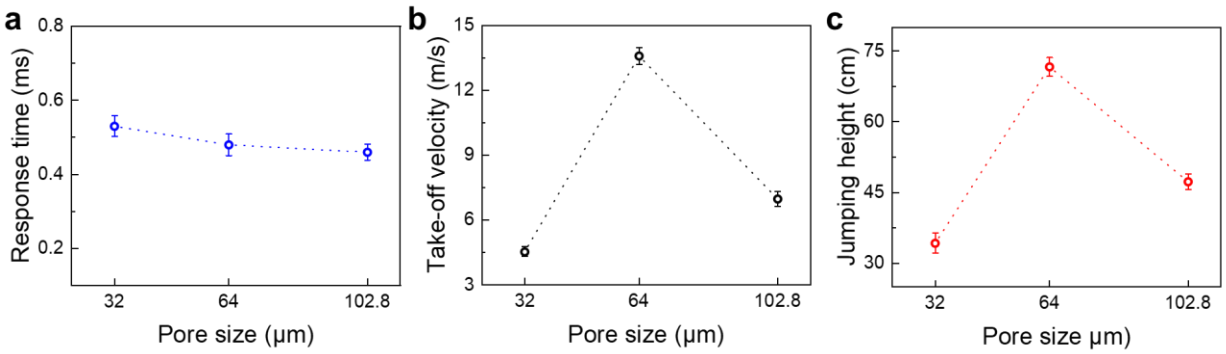

Supplementary Figure 33. The influence of the surface pore size on (a) the response time, (b) the take-off velocity and (c) the jumping height of the light-driven jumper. Error bars denote the standard deviation.

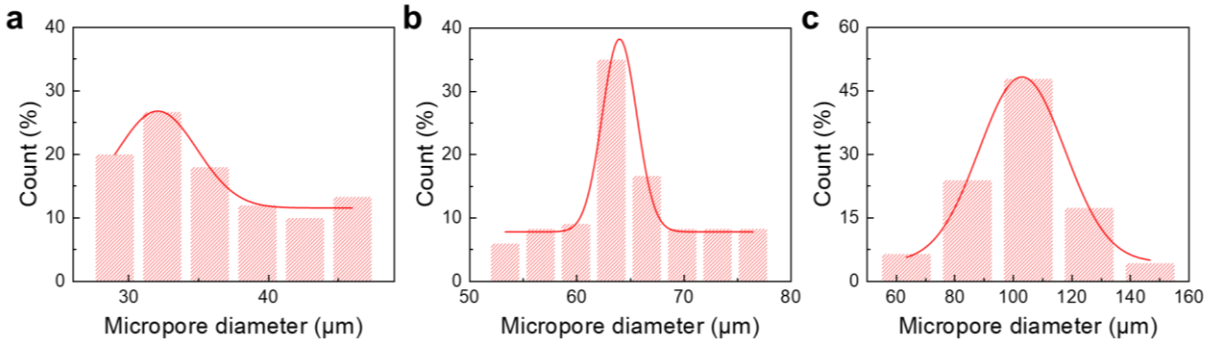

Supplementary Figure 34. (a-c) The micropore size distributions of the light-driven jumpers with average pore diameters of 32 μm, 64 μm, and 102.8 μm, respectively.

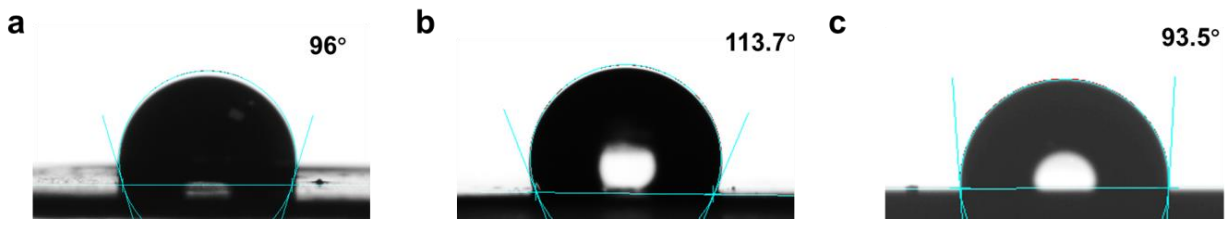

Supplementary Figure 35. CCD images showing the water contact angles on the surface of the light-driven jumper with surface pore size of (a) 32 μm, (b) 64 μm, and (c) 102.8 μm, respectively.

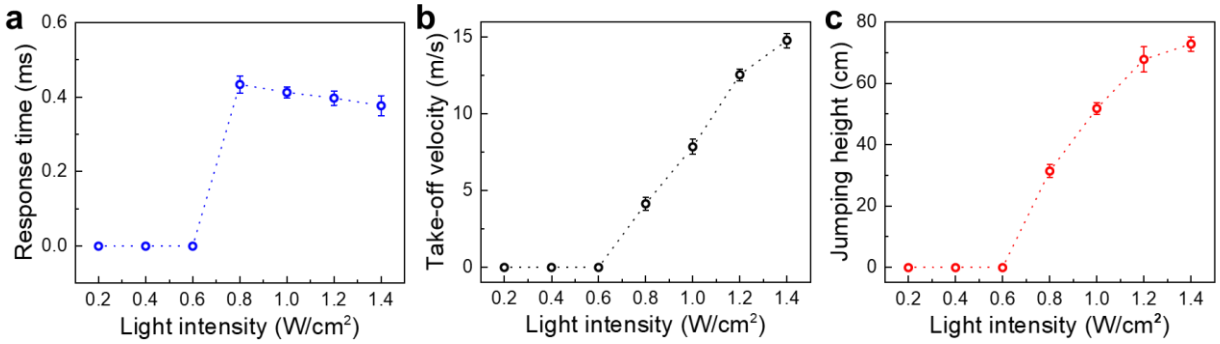

Supplementary Figure 36. The effect of the irradiation light intensity on (a) the response time, (b) the take-off velocity and (c) the jumping height of the light-driven jumper. Error bars denote the standard deviation.

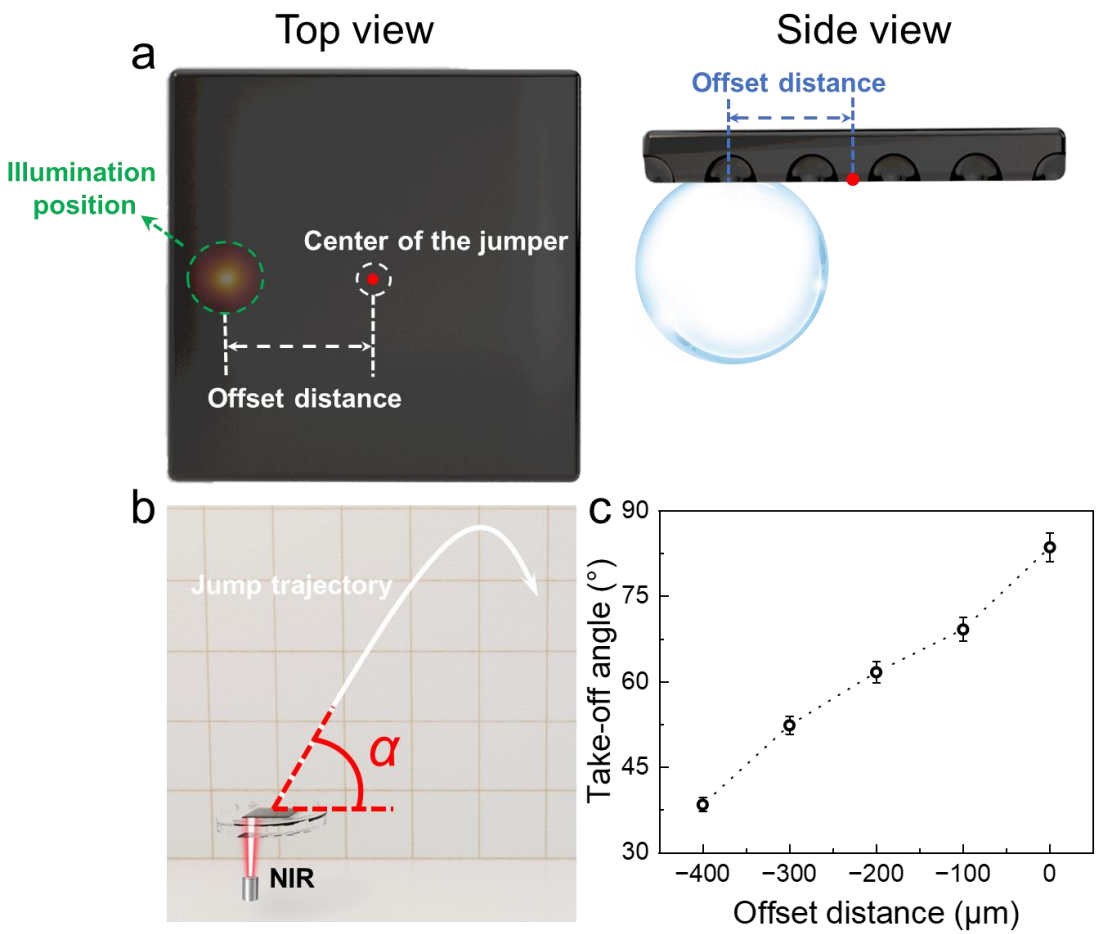

Supplementary Figure 37. Schematic showing (a) the offset distance of the illumination spot from the jumper's center and (b) the take-off angle of the (α) jumper. (c) The effect of the distance between the illumination position and the center of the light-driven jumper on the take-off angle. Error bars represent standard deviations.

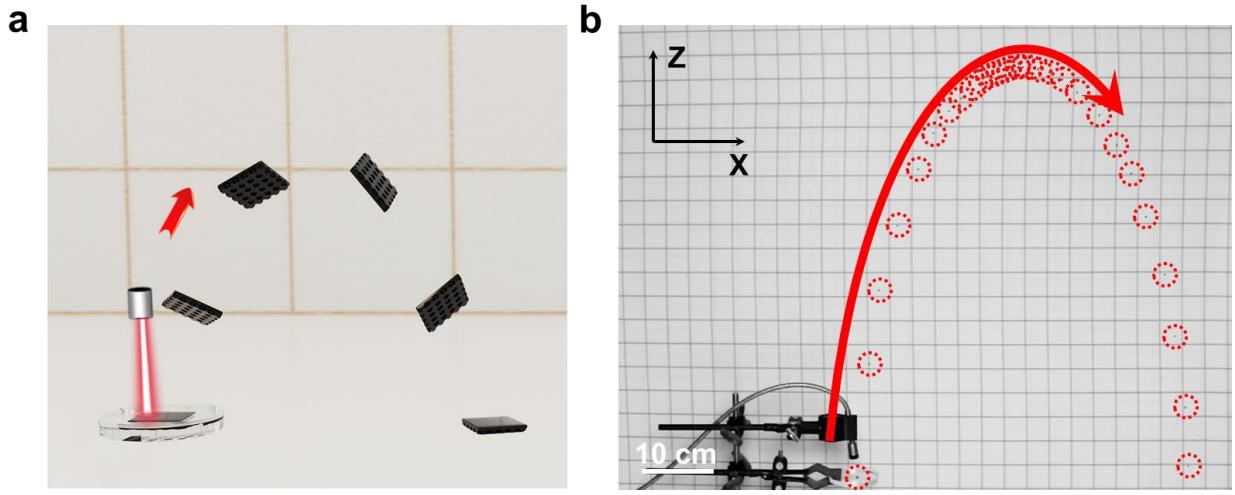

Supplementary Figure 38. (a) Schematic illustration and (b) overlaid CCD images showing the water-surface jumping behavior of the light-driven jumper under top illumination, with the red curve denoting the jumping trajectory and red dashed circles marking its positions at different periods of time (~0.017 s).

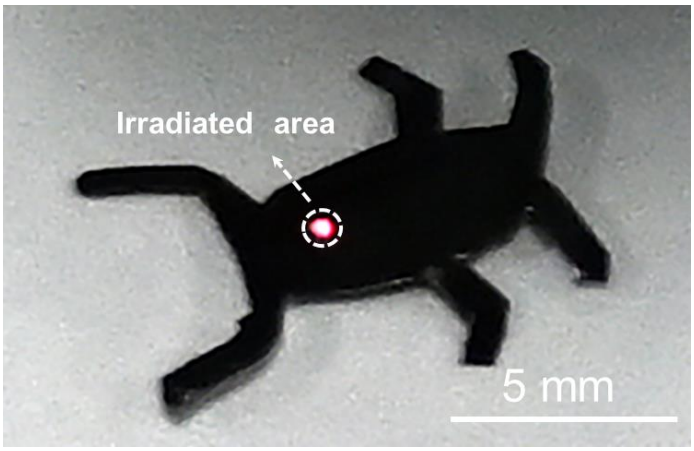

Supplementary Figure 39. CCD image showing the size of the light spot relative to that of the artificial water strider.

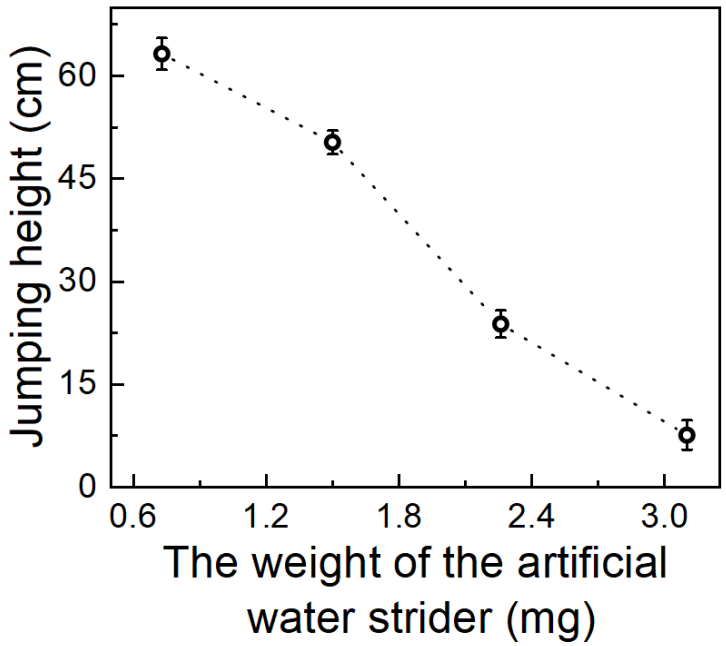

Supplementary Figure 40. The influence of the weight of the artificial water strider on its jumping height. Error bars denote the standard deviation.

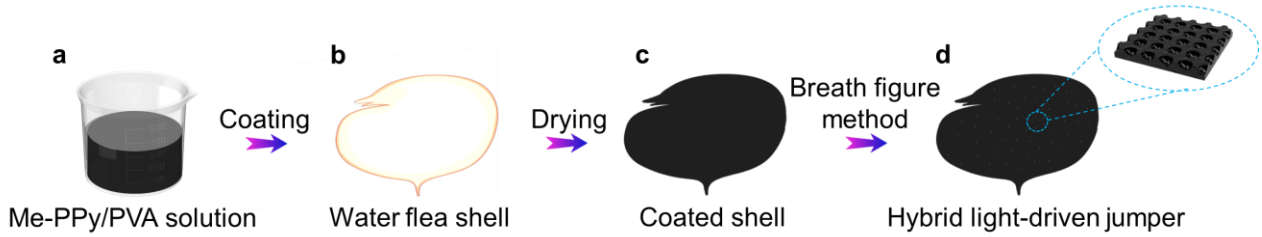

Supplementary Figure 41. (a-d) Schematics illustrating the fabrication process of the hybrid light-driven jumper by coating the shell of a water flea with the Me-PPy/PVA composite.

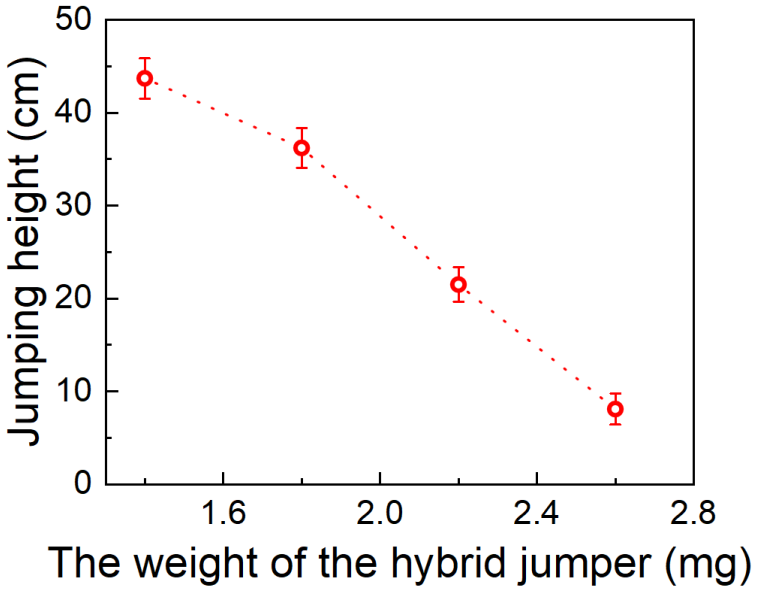

Supplementary Figure 42. The influence of the weight of the hybrid jumper on the jumping height. Error bars denote the standard deviation.

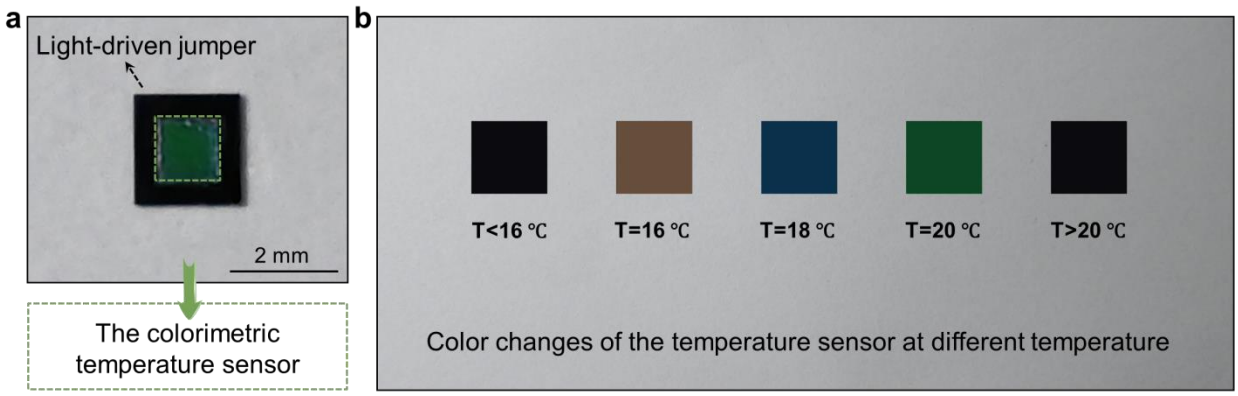

Supplementary Figure 43. (a) CCD image showing the light-driven jumper integrated with a colorimetric temperature sensor. (b) Color changes of the temperature sensor at different temperatures.

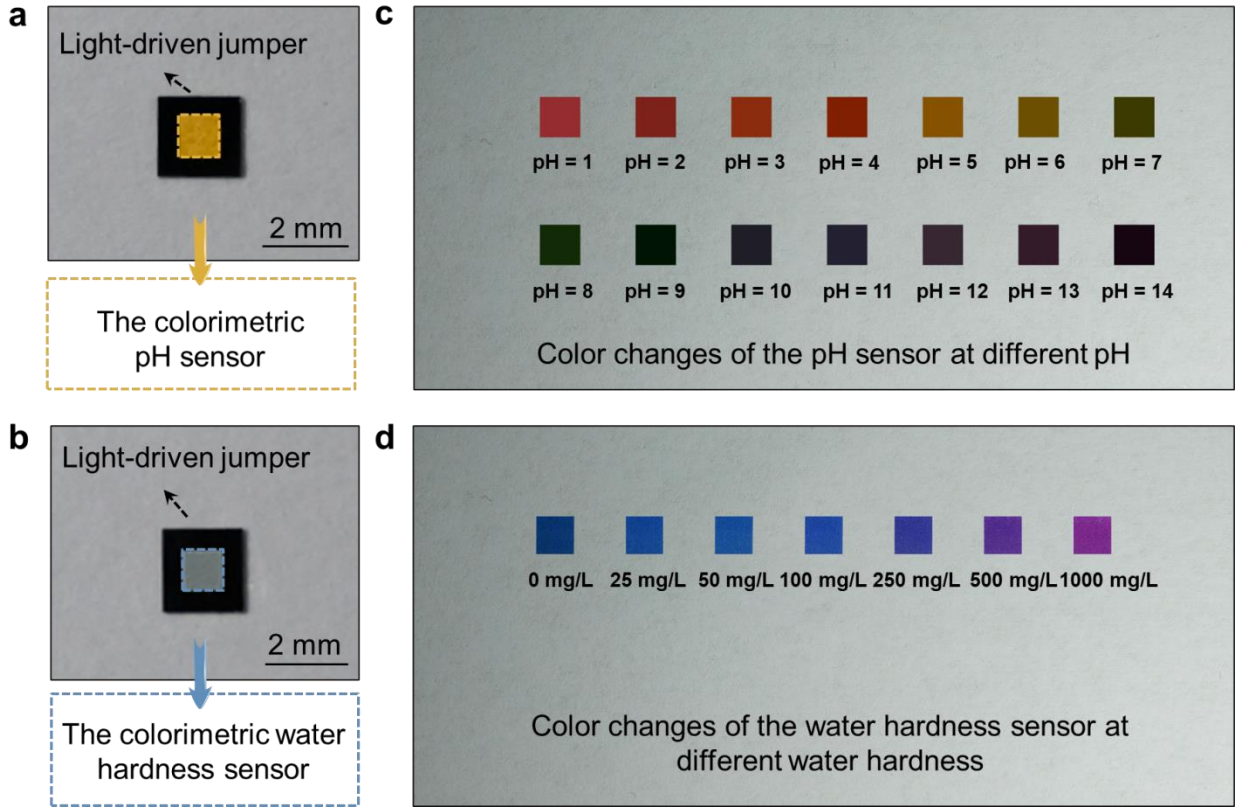

Supplementary Figure 44. CCD images showing light-driven jumpers integrated with (a) colorimetric pH and (b) water hardness sensors, respectively. Color changes of (c) the pH and (d) water hardness sensors at different pH and water hardness, respectively.

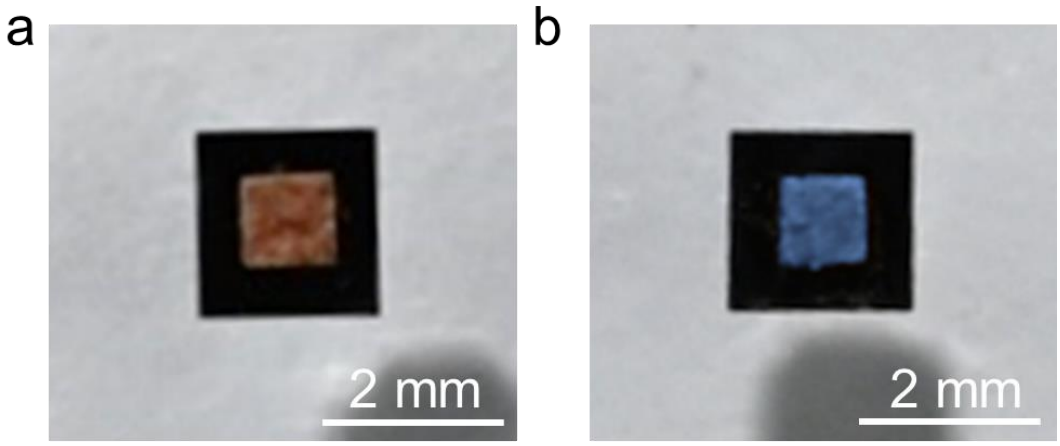

Supplementary Figure 45. CCD images of the light-driven jumper integrated with (a) the colorimetric pH or (b) water hardness sensor, showing the color changes 5 min after reaching the target water region.

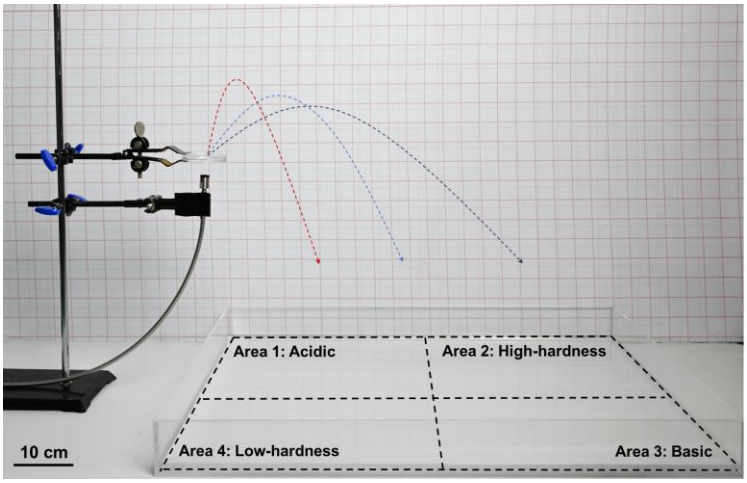

Supplementary Figure 46. CCD image showing the experimental setup for the collective water environment sensing. The four areas (from 1 to 4) represent acidic, high-hardness, basic, and low-hardness water environments, respectively.

Supplementary Reference

1. Burrows M & Sutton GP. Pygmy mole crickets jump from water. *Curr. Biol.* **22**, R990-R991 (2012).
2. Ortega-Jimenez VM, et al. Directional takeoff, aerial righting, and adhesion landing of semiaquatic springtails. *Proc. Natl. Acad. Sci. U.S.A* **119**, e2211283119 (2022).
3. Suter RB & Gruenwald J. Predator avoidance on the water surface? Kinematics and efficacy of vertical jumping by dolomedes (Araneae, Pisauridae). *J. Arachnol.* **28**, 201-210 (2000).
4. Song Y, Wang H, Dai Z, Ji A, Wu H & Gorb SN. Multiple forces facilitate the aquatic acrobatics of grasshopper and bioinspired robot. *Proc. Natl. Acad. Sci. U.S.A* **121**, e2313305121 (2024).
5. Kim W, et al. Two different jumping mechanisms of water striders are determined by body size. *Proc. Natl. Acad. Sci. U.S.A* **120**, e2219972120 (2023).

Supplementary Movies

Supplementary Movie 1.
The water surface jumping behavior of the light-driven jumper captured by the high-speed camera.

Supplementary Movie 2.
The jumping motion of the light-driven jumper with a jumping height of 72.8 cm.

Supplementary Movie 3.
The bubble formation, growth and burst processes captured by high-speed camera.

Supplementary Movie 4.
The light-driven jumper jumping to the right.

Supplementary Movie 5.
The light-driven jumper jumping to the left.

Supplementary Movie 6.
The water surface jumping motion of the artificial water strider.

Supplementary Movie 7
Water surface jumping motion of the hybrid light-driven jumper.